Dynamic Analysis of Multihazard-Resistant Bridge Piers Having Concrete-Filled Steel Tube under Blast Loading

Shuichi Fujikura, M.ASCE[1] and Michel Bruneau, F.ASCE[2]

Abstract: Research was conducted to analytically investigate the blast-response and behavior of multihazard-resistant bridge piers having circular-shaped, concrete-filled steel tube (CFST) columns. Two different analysis methods, namely a single-degree-of-freedom (SDOF) dynamic analysis and a fiber-based dynamic analysis, were used for this purpose and calibrated with the maximum residual deformations obtained from 1/4 scale blast tests of CFST columns. It was noted that the structural response of SDOF dynamic analyses is sensitive to assumptions made in the load-mass factors needed to model structural components as an equivalent SDOF system. Fiber-based dynamic analyses showed that high-frequency modes of vibration have some influence on the structural response when subjected to blast loading. This study shows that different values of the shape factors, β (which reduces blast pressures when applied to a circular column), must be used with different analytical methods, along with assumptions and conditions behind these different analytical methods. **DOI: 10.1061/(ASCE)BE.1943-5592.0000270.**

CE Database subject headings: Blast loads; Bridges; Piers; Columns; Steel; Dynamic analysis.

Author keywords: Blast loads; Bridges; Piers; Columns; Steel; Concrete-filled steel tube; Dynamic analyses; Multi-hazard.

Introduction

The authors previously presented a multihazard-resistant bridge pier concept, more specifically, a multicolumn pier-bent concept relying on concrete-filled steel tube (CFST) columns, to provide seismic and blast resistance. The performance of this system was experimentally investigated under blast loadings (Fujikura et al. 2007, 2008). From test observations, the blast performance of this system was shown to be superior, by contrast, to that of comparable seismically ductile RC columns and nonductile RC columns retrofitted with steel jackets (Fujikura and Bruneau 2011). In fact, seismically ductile RC columns and steel jacketed nonductile RC columns of comparable strength were not found to exhibit a ductile behavior when subjected to blast loading but failed in direct shear at their base.

Along with the blast tests on the proposed CFST bridge pier columns, a simplified analysis procedure was also presented to calculate the maximum deformation of CFST columns by considering a shape factor, β, to account for the reduction of pressures on circular columns due to the shape of the column. However, to better understand the behavior of this system subjected to blast loading, more advanced dynamic analysis is required. It is the purpose of this paper to present the results of such relatively more sophisticated analyses and to use the results of these analyses to help understand the behavior of these circular-shaped CFST bridge columns that developed ductile flexural hinges when subjected to blast loading [note that columns that fail in direct shear, such as those reported by Fujikura and Bruneau (2011), are beyond the scope of this paper].

There is a variety of analytical methods available to compute the response of structures subjected to blast loading, ranging from simplified analysis models to finite element models (FEMs). In light of the objectives for the dynamic analyses conducted here, two different analytical methods have been adopted to replicate the behavior of the tested CFST columns subjected to blast loading, namely a single-degree-of-freedom (SDOF) dynamic analysis and a fiber-based dynamic analysis. The maximum residual deformations obtained from these two blast dynamic analyses are compared with the experimental results. Additionally, these analysis results are compared with the ones from simplified analyses conducted using an equivalent SDOF system, presented previously (Fujikura et al. 2007, 2008).

The analyses are also used to revisit the shape factor β. Introduced previously for use with the simplified analysis method, this factor is unavoidably affected by analysis assumptions. When a more sophisticated analytical model is used, some of these assumptions are removed, and it would be incorrect to use the same β value as developed for the simplified method. Therefore, the factor β is reevaluated to be compatible with the advanced analysis methods.

Note that since the β factor in its purest form is a function of load effects, ideally it should be calculated using the measured pressures all around the column; interaction of a shock wave with a cylindrical object is a complicated process, due to the Mach stem, vortices, and region of supersonic flow around the object (Baker 1973), and calculating the loads imposed to a cylindrical column would require using pressure transducers all around the column (and along its height for close-range blasts). However, it was not possible to reliably measure the pressures considered in these close-range blast tests because of turbulence issues at such close distances to the charge and because of limits in pressure gage capabilities. Therefore, the approach taken here was to use the column specimens, which are ductile and have the ability to flex plastically, as a displacement-measuring instrument to predict the impulse applied to the column, by back-calculating this value from the plastic

[1]Structural Engineer, Buildings Sector, Arup North America, Los Angeles, CA 90066 (corresponding author). E-mail: shuichi.fujikura@arup.com

[2]Professor, Dept. of Civil, Structural, and Environmental Engineering, Univ. at Buffalo, Buffalo, NY 14260. E-mail: bruneau@buffalo.edu

Note. This manuscript was submitted on April 30, 2010; approved on May 10, 2011; published online on May 12, 2011. Discussion period open until August 1, 2012; separate discussions must be submitted for individual papers. This paper is part of the ***Journal of Bridge Engineering***, Vol. 17, No. 2, March 1, 2012. ©ASCE, ISSN 1084-0702/2012/2-249–258/$25.00.

deformation of the column. Depending on its deformation after the blast test, the impulse can be calculated by assuming that all the energy imparted to the system by the blast loading is converted into internal strain energy.

Multihazard-Resistant Bridge Pier Tests Subjected to Blast Loading

Preliminary analyses predicted that CFST bridge piers would exhibit high resistance and ductility against both blast and seismic loads. To verify/validate performance for the first of these two hazards, a series of blast tests of 1/4 scale bridge piers was performed at the U.S. Army Corps of Engineers Research Facility in Vicksburg, Mississippi (Fujikura et al. 2007, 2008). Two identical specimens (Bent 1 and Bent 2) were constructed and tested. Each specimen consisted of three CFST columns with different diameters: $D = 102$ mm (4 in.), 127 mm (5 in.), and 152 mm (6 in.), connected to a steel beams embedded in the cap beam and foundation beam (Fig. 1). A summary of the experimental cases and test results is presented in Table 1. Exact values of charge weights and standoff distances are normalized and expressed in functions of W and X, respectively, for security reasons. Note that each column in the bent was tested successively as if it was a part of a regular bent. The CFST columns exhibited a ductile behavior under blast loadings, and the experimentally obtained maximum residual deformations of the columns are presented in Table 1.

Table 1. Summary of Blast Tests

		Blast parameters			Test results
Test number	Column	w	x	z (m)	Residual displacement (mm)
1	C4	0.1 W	3 X	0.25	0
2	C4	0.55 W	3 X	0.75	0
3	C4		2 X		30
4	C6		1.1 X		46
5	C5		1.3 X		76
6	C4		1.6 X	0.25	24
7	C4	W	0.6 X		395
9	C6		0.8 X		45
10	C5		0.8 X		100

Comparison of Analytical Methods

There is a variety of analytical methods available to compute structural response subjected to blast loading, ranging from simplified analysis using a SDOF system to FEM that replicates the detailed structural elements and materials and that accounts for the actual blast pressure histories acting on the structure. Table 2 summarizes some of the analytical options available to compute the response of structures subjected to blast loading. Winget et al. (2005) provided a good overview of various analytical options by comparing their advantages and disadvantages.

As mentioned earlier, a SDOF dynamic analysis and a fiber-based dynamic analysis have been adopted here to replicate the behavior of the tested columns under blast loading, and these results are compared with the ones from the simplified analysis presented previously. Note that there exist more complicated analytical approaches using finite element analysis packages, such as LS-DYNA (Livermore Software Technology Corp.) and AUTODYN (Century Dynamics, Inc.), that can model fluid-structural interaction. However, these are beyond the reach of most bridge engineers. The scope of the study here is limited to using analytical models that are compatible with what most bridge engineers are already familiar with.

The common aspects of the three analytical methods adopted here (as outlined in Table 2) are that (1) they are dynamic analyses, (2) the structure and the blast loading are uncoupled, (3) material nonlinearity is considered, and (4) geometric nonlinearity is not considered. Uncoupled analysis is chosen here, because it is commonly used in the practical design of structures under dynamic loading and provides reasonable results (Winget et al. 2005). The material nonlinearity is considered here because all materials

Table 2. Options for Blast Resistance Analysis

Modeling	Analytical options
Consideration of blast pressures	(a) Equivalent static analysis; (b) dynamic analysis
Interaction between structure and blast loading	(a) Coupled analysis; (b) uncoupled analysis
Discretization of structure	(a) SDOF model; (b) MDOF 2D or 3D beam model; (c) MDOF FEM
Material nonlinearity	(a) Elastic model; (b) inelastic model
Geometric nonlinearity	(a) Linear model; (b) nonlinear model

Note: MDOF = multidegree-of-freedom.

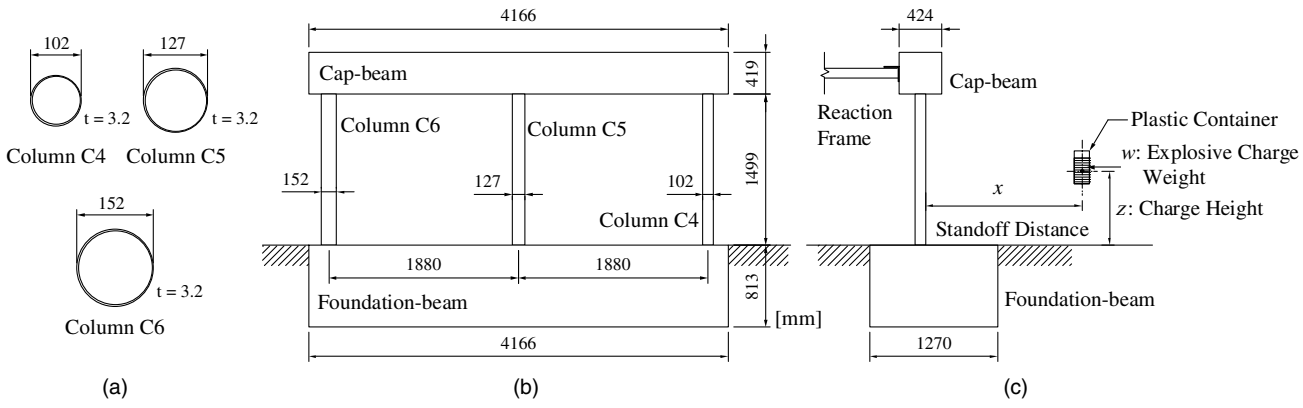

Fig. 1. Experimental specimens and explosive charge scenario

behaved in the inelastic range under the blast pressures considered in this research, but the geometric nonlinearity was not considered. The blast tests were conducted without axial forces applied to the columns (except for the gravity load of the cap beam), but the $P-\delta$ effect was considered separately. $P-\delta$ analyses showed that the columns would have remained stable at all times under the magnitude of axial loads typically expected to be present in such columns. Note that the $P-\delta$ analyses conducted here were for investigating whether the deformed column would buckle due to the gravity load of the superstructure after the blast. Dynamic global buckling of the columns was not an issue in these specific experiments, because dynamic buckling strength is higher than static buckling strength in these cases (however, note that dynamic buckling strength depends on the dynamic characteristics of the input loads and can, in some instances, be less than static buckling strength). Incidentally, during the blast itself, given that the charge would be detonated under the bridge deck, uplift pressures on the superstructure would temporarily reduce the axial load on the column, further lessening dynamic buckling concerns.

The main differences between the three analysis methods considered here are that the dynamic load is applied differently and the structure is discretized differently. The simplified analysis uses the concept of equivalent impulse to calculate the maximum deformation, assuming that all the energy imparted to the system by the blast loading is converted into internal strain energy. This analytical method provides acceptable results when the blast pressure duration is much shorter than the natural period of the structure (i.e., impulsive loading condition). The SDOF dynamic analyses and fiber-based dynamic analyses are conducted using the equivalent uniform pressure history and the actual pressure history, respectively; such distributions can be generated by various software, such as the program Bridge Explosive Loading (BEL) Version 1.1.03 used in this research. As for model discretization, the simplified analysis and the SDOF dynamic analysis use the same SDOF lumped-mass system (equivalent SDOF system), whereas the columns are modeled by a two-dimensional (2D) fiber-based beam model in the fiber-based dynamic analysis.

Experimentally obtained maximum residual deformations of the tested columns are compared with the ones that could be calculated using the three different analyses. These analyses were conducted for the six test cases of CFST columns for which residual plastic deformations were obtained (as presented in Table 1). The strength values obtained from the compression tests of concrete cylinders and the tensile tests of coupons taken from the steel tubes were considered in these analyses. Material properties depend on strain rates, and the strength typically increases with the strain rate. However, for expediency, the concrete strength and yield stress of steel were simply multiplied by 1.25 and 1.2, respectively, to account for this strength magnification at large strain rates under impulsive conditions (Mays and Smith 1995).

SDOF Dynamic Analysis

There are a few programs available to perform a SDOF dynamic analysis for structures subjected to blast loading, such as the program SPAn32 Version 1.2.7.2, whose distribution is limited to the U.S. government agencies and their contractors, and the program NONLIN Version 6.01, which is a public domain program originally developed for seismic response time-history analyses of SDOF systems. However, here, the program Single-Degree-of-Freedom Blast Effects Design Spreadsheets (SBEDS) Version 3.1, which is a product of the U.S. Army Corps of Engineers, was used because its distribution is unlimited for public use and this program is tailored for blast engineering design rather than earthquake engineering design. SBEDS is typically used to design structural components subjected to blast loading, using an equivalent SDOF model, and is structured to run on an Excel workbook platform. A user-defined pressure history can also be incorporated in the analysis (USACE 2006).

SDOF Dynamic Analytical Model

The equation of motion for an equivalent SDOF system in blast applications is often written as (Biggs 1964; USACE 2006):

$$K_M M\ddot{x} + K_D C\dot{x} + K_L K x = K_L P(t) \tag{1}$$

where M, C, K, and $P(t)$ = mass, viscous damping, stiffness, and load of the real structure, respectively; and K_M, K_D, and K_L = mass, damping, and load factors, respectively. The factors that transform the continuous system into an equivalent SDOF one are

$$K_M = \frac{M_e}{M_t} = \frac{\int_0^L m\phi^2(x)dx}{mL} \tag{2a}$$

$$K_L = \frac{F_e}{F_t} = \frac{\int_0^L p(x)\phi(x)dx}{pL} \tag{2b}$$

where m, p, L, $\phi(x)$, and $p(x)$ = mass per unit length, load per unit length, span length, assumed shape function of the structure, and applied load function, respectively. For expediency, the equation of motion of the real structural system is expressed as a SDOF system that only depends on a load-mass factor, $K_{\mathrm{LM}} = K_M/K_L$, such that

$$K_{\mathrm{LM}} M\ddot{x} + C\dot{x} + Kx = P(t) \tag{3}$$

and assuming that $K_L = K_D$ (USACE 2006). This is not necessarily correct mathematically, but it is an approach that has been commonly used in blast engineering and the one used in SBEDS (USACE 2006). Note that the simplified analytical method used previously (Fujikura and Bruneau 2008) neglected the damping term, because only one cycle of structural response develops under blast loading and because that method cannot take damping into account.

The load-mass factor, K_{LM}, depends on boundary conditions and loading conditions (Biggs 1964). Furthermore, for the same given boundary condition and loading condition, the load-mass factor, K_{LM}, for the specific structure can take different values depending on whether the structure behaves in the elastic, elastoplastic, or plastic ranges. This is because virtual work developed in the element depends on the element deformation shape, which is different in each range. A fixed-fixed boundary condition and a uniformly distributed load were chosen for the experimental columns. These boundary conditions are representative of what was observed in the experiments due to the torsional resistance of the cap beam. For this fixed-fixed boundary condition and a uniformly distributed load, the corresponding load-mass factors, K_{LM}, are 0.77, 0.78, and 0.66 for response in the elastic, elastoplastic, and plastic ranges, respectively.

The simplified analysis uses the idealized bilinear resistance-displacement relationship to consider inelastic behavior of a column. Even though the dynamic SDOF analyses conducted using SBEDS can handle a trilinear resistance curve (as well as more complex ones), for the sake of comparing the dynamic analysis results with the simplified analysis results, it was decided to use the same equivalent resistance-displacement function as in the simplified analysis. In this equivalent resistance function, since the program SBEDS can assign different load-mass factors to different

ranges, the load-mass factor, K_{LM}, of 0.775 was taken as the average value of the elastic and elastoplastic ranges and of 0.66 for the plastic range. Note that, in the simplified blast analysis, the value of 0.66 was used for the load-mass factor because only one value could be considered in that analysis and the test columns deformed in large plastic deformations. For comparison purposes, the following analyses will investigate the influence of assumptions related to this load-mass factor on the structural responses (note that how the factor itself impacts structural response is well known, it being a function of stiffness and mass; it is the impact of various modeling assumptions that is of interest here).

The uniformly distributed load corresponding to ultimate resistance of a column, r_u, is calculated assuming that plastic hinges form at the top and base of a column, as well as at the explosion height (as demonstrated to be the case experimentally), and is given by $r_u = 12M_p/L^2$ for midheight explosion cases and by $r_u = 28.8M_p/L^2$ for low-height explosion cases for which the charge was at 0.25 m high. M_p is the plastic moment capacity of a column, which was calculated using the equation presented by Bruneau and Marson (2004) and recently adopted by AASHTO (2009). The resulting plastic moment capacity, M_p, of the column specimens was 15.1, 16.5, and 40.5 kN-m for Columns C4, C5, and C6, respectively. An equivalent maximum elastic deformation, X_E, is given by $X_E = r_u/K_e$ where K_e, the unit elastic stiffness of an equivalent SDOF system, is given by $K_e = 307EI_e/L^4$ (Mays and Smith 1995). The flexural stiffness of a column, EI_e, was calculated using the equation introduced in Eurocode 4 (Commission of the European Communities 1994) because the AISC provisions (AISC 1999) do not provide an equation for EI_e (Bruneau and Marson 2004). The resulting design values used for the SBEDS analyses are summarized in Table 3. Note that these values are presented in unit per area (rather than for the element as a whole), per SBEDS requirements.

Table 3. Summary of Design Values for SDOF Dynamic Analyses

	SDOF dynamic analysis		
Test number	Mass per m/D (kg/m^2) unit area	Stiffness per unit area K_e/D (kPa/mm)	Resistance per unit area r_u/D (kPa)
3	243.7	192.2	1,062.0
4	340.0	538.9	1,892.2
5	291.9	322.6	924.9
6	243.7	192.2	1,911.1
9	340.0	538.9	3,404.7
10	291.9	322.6	1,664.5

Note: D = column diameter.

Applied Blast Loading

The blast pressures acting on a column vary with time and locations along the column. In the simplified analysis, a single value of an equivalent uniform impulse was needed to calculate the maximum response of a column modeled as a SDOF system. The envelope of the maximum impulse along a column was used to calculate this equivalent uniform impulse (Fujikura et al. 2007, 2008). In the SDOF dynamic analysis, a single value of an equivalent uniform pressure at a given time is applied to the structural model following a time-history, step-by-step analysis. This equivalent uniform pressure at time of t, $p_{eq}(t)$, is given by

$$p_{eq}(t) = \frac{\int_0^H p(z,t)\phi(z)dz}{\int_0^H \phi(z)dz} \tag{4}$$

where $p(z,t)$ = pressure distribution along the height of a column at time t. The values of $p(z,t)$ were calculated using BEL, which was also used for the simplified analyses. The normalized deflected shape, $\phi(x)$, was taken as inelastic deformations after plastic hinging. The shape was defined by rigid-link members between plastic hinges assuming that an in-span hinge develops at the height of a blast charge and that other hinges form at both the top and base of a column. Note that the equivalent uniform pressure, $p_{eq}(t)$, calculated by Eq. (4), takes pressure variation along a column into account based on the deflected shape of the column, $\phi(x)$. The resulting equivalent pressure history, $p_{eq}(t)$, for Test 3 on Column C4 is shown in Fig. 2(a) as an example. The time increment of each step in the pressure histories is 0.01 ms.

SDOF Dynamic Analysis Results

The sensitivity of assumptions made with respect to the load-mass factors, K_{LM}, and damping effects on the structural response was investigated in order to see which values would be more appropriate for the load-mass factors in the elastic and plastic ranges and for the viscous damping ratio. This is done below using Test 3 on Column C4 as a typical case for illustration purposes. In the simplified analytical procedure, the damping effect was not considered, and the load-mass factor, K_{LM}, was assumed to be 0.66. For comparison, four SDOF dynamic analyses were conducted, considering viscous damping ratios of 0 and 5%, and various values of load-mass factors over different ranges of response (which SBEDS is able to take into account). Case 1 considers the same load-mass factors and viscous damping ratio as those considered in the simplified analysis, namely $K_{LMe} = K_{LMp} = 0.66$ and no damping, where K_{LMe} and K_{LMp} = load-mass factor for the elastic and plastic range, respectively, such as to replicate the results of the simplified

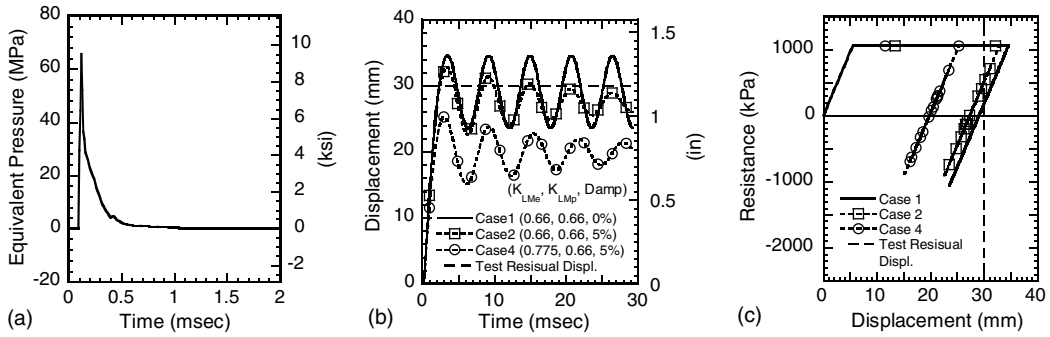

Fig. 2. Applied pressure and analytical results of SDOF dynamic analysis (Test 3 on Column C4 with $\beta = 0.472$): (a) equivalent pressure history; (b) displacement response; (c) resistance-displacement relationship

analysis with the dynamic simplified analysis. Case 2 is identical to Case 1, except that it considers a viscous damping ratio ξ of 5%. Cases 3 and 4 consider the appropriate load-mass factors over the different ranges of structural response, namely K_{LMe} and K_{LMp} of 0.775 and 0.66, respectively. The viscous damping ratio ξ of Cases 3 and 4 are 0 and 5%, respectively.

The analytical results of the displacement history and resistance-displacement relationship obtained for Cases 1, 2, and 4 are shown in Figs. 2(b) and 2(c), respectively, when the shape factor β is taken as 0.472, that being the value resulting from the simplified analysis for this particular column case reported by Fujikura et al. (2007, 2008). Note that the resistance in Fig. 2(c) is expressed in a unit of pressure (kPa) because the program considers the structure per unit area. The dashed line at 30 mm in these figures shows the maximum residual displacement obtained from the experiment. The displacement when resistance equals zero (after the structure has been loaded and unloaded) in Fig. 2(c) is the residual plastic displacement that should be equal to the experimentally obtained residual displacement of 30 mm, in this case. By comparing displacement history curves of Cases 1 and 2 in Fig. 2(b), it can be seen that the consideration of damping effect has a small effect on response, with an approximate 5% reduction of the maximum deformation reached. However, the curve considering damping shows the progressive attenuation of the amplitude of vibrations. More importantly, comparing the displacement history curves of Cases 2 and 4 in Fig. 2(b), the use of two values of load-mass factor, K_{LM}, in Case 4 resulted in a 23% reduction of the maximum displacement amplitude. Therefore, this factor has a more significant impact on the maximum displacement. These impacts can also be seen in the residual displacement results shown in Fig. 2(c).

To match the analytical residual displacements with the experimental results, the shape factor β was calibrated for the six tested CFST columns. Table 4 summarizes the average values of resulting shape factors β for midheight explosion cases (Tests 3–5), low-height explosion cases (Tests 6, 8, and 10), and all six cases, including the ones obtained from the simplified analyses and fiber-based analyses (to be presented in the next section). Note that the larger the shape factor, the larger the blast pressures that the structure can resist. It is observed from Table 4 that the value of β is about 4% less for low-height explosions than midheight ones. Since the height of an explosion does not have a significant impact on the value of β, the average values of β for all columns are compared between the cases. Note that the shape factors obtained from the simplified analysis and from Case 1 compare within 1%. This confirms that the simplified analysis based on energy conservation is equivalent to the SDOF dynamic analysis under the same conditions of load-mass factor and the damping ratio (i.e., $K_{LM} = 0.66$ and $\xi = 0\%$, in this case). Using a 5% viscous damping ratio slightly reduces structural response and thus slightly increases the factor β required to obtain the same residual deformation, which can be observed by comparing the shape factor obtained from Cases 1 and 2 and from Cases 3 and 4. The difference is within 3%. In Cases 3 and 4, using the load-mass factor in the elastic range, K_{LMe}, of 0.775, in addition to that over the plastic range of 0.66, increases the shape factor by approximately 15% over that for Cases 1 and 2, respectively, which shows that assumptions made with respect to the load-mass factor have a significant impact on the structural response in the SDOF dynamic analysis.

Fiber-Based Dynamic Analysis

Fiber-based dynamic analyses were conducted to better understand the behavior of tested CFST columns when subjected to blast loading. Although an advanced FEM using solid elements or shell elements might be appropriate for capturing the localized behavior of the structural elements such as beam-column connections, frame models using a fiber-based model are more computationally effective to accurately capture the nonlinear dynamic response of structures (Spacone et al. 1996a, 1996b). In the fiber-based model, a member section is divided into fibers in which the unidirectional stress-strain relationships of materials are assigned to represent the section characteristics, and the fiber-based model assumes that a plane section remains plane. The open-source OpenSees Version 1.7.5 program was used to perform the fiber-based analyses in this research. Note that the fiber-based model is suitable to capture flexural and axial behavior of the structure but it cannot capture shear failure of the type observed in the previous tests of ductile reinforced concrete columns and steel jacketed nonductile reinforced concrete columns (Fujikura and Bruneau 2011). None of the tested CFST columns considered here failed in shear, mostly due to the high shear capacity of steel tubes that are an integral part of CFST columns; rather, they failed in flexure. Therefore, using fiber-based analysis is a suitable approach to capture the residual plastic displacement observed during the test program.

Fiber-Based Analytical Model

Fig. 3 schematically shows the fiber-based analytical model of CFST columns for the blast loading tests. As shown in Fig. 3(a), the sections are divided into fibers for which the different materials are assigned different unidirectional stress-strain relationships. For a typical CFST, the steel tube was modeled as 64 discretized steel bar fibers, and the core concrete was modeled by 256 concrete fibers. The Menegotto-Pinto uniaxial constitutive model (Menegotto and Pinto 1973) was used for steel tubes. This model considers the hysteretic behavior of steel and accounts for the Bauschinger effect. Core concrete was modeled using the Chang and Mander (1994) confined concrete model, modified by J. Waugh (personal communication, 2007) to increase its computational efficiency and numerical stability. Bruneau and Marson (2004) showed that the confined concrete strength calculated by

Table 4. Summary of Shape Factors from SDOF Dynamic Analyses and Fiber-Based Dynamic Analyses

	Simplified analysis	SDOF dynamic analysis				Fiber-based analysis		
		Case 1	Case 2	Case 3	Case 4	UD equivalent pressure		Actual pressure
Analysis	$K_{LMe} = 0.66$	0.66	0.66	0.775	0.775	Not available	Not available	Not available
Parameters	$K_{LMp} = 0.66$	0.66	0.66	0.66	0.66	Not available	Not available	Not available
	$\xi = 0\%$	0%	5%	0%	5%	0.5%	5%	5%
Midheight	0.459	0.463	0.472	0.532	0.542	0.547	0.643	0.665
Low height	0.441	0.442	0.453	0.510	0.525	Not available	Not available	0.561
Total average	0.450	0.453	0.463	0.521	0.534	Not available	Not available	0.613

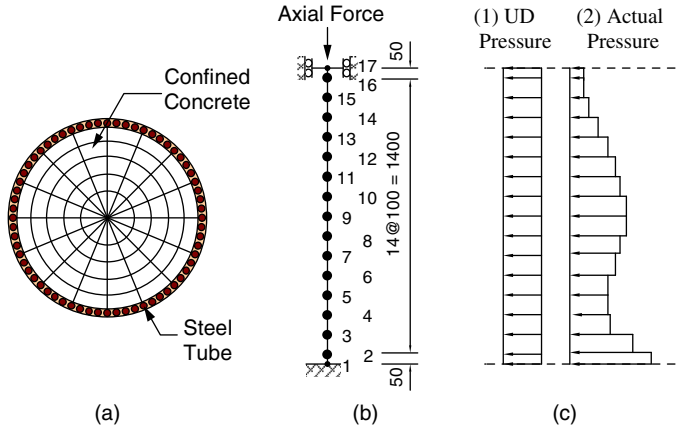

Fig. 3. Analytical model for blast loading tests: (a) cross section for fiber elements; (b) discretized model; (c) applied loading

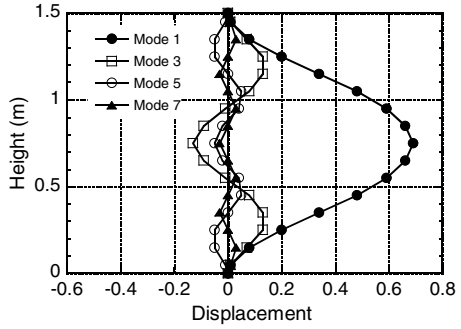

Fig. 4. Natural mode shapes of Column C4

considering all the steel tube as concrete confinement significantly overestimates the capacity of CFSTs. Therefore, the effective confinement stress, f'_l, was taken as 2.07 MPa (300 psi), which is the value used in the design of steel jacketed RC columns (Chai et al. 1991). The columns were modeled as discrete frames, as shown in Fig. 3(b). Discrete lumped masses were assigned to Nodes 2–16 as inertias to resist the blast loads. The gravity load corresponding to these masses was applied as a uniformly distributed load along column height. An axial force of 5.81 kN (1.31 kip) was applied to consider the loading from the cap beam.

Damping effects were considered through Rayleigh damping of 5%. Modal analyses were conducted for the three CFST columns with different diameters (Columns C4, C5, and C6) to determine two modes of vibration for Rayleigh damping, and also to investigate their vibration properties, namely natural periods and mode shapes. The natural mode shapes of Modes 1, 3, 5, and 7 for Column C4 are shown in Fig. 4. These mode shapes are normalized by their corresponding effective masses. Note that because of fix-fix boundary conditions of the columns, antisymmetric modes (such as Modes 2, 4, and 6) do not contribute the structural responses. Since, as shown in Fig. 4, Modes 1 and 3 are the dominant modes whose effective masses are, respectively, 69.0 and 13.2%, Rayleigh damping was specified by these two modes. The vibration properties of Columns C5 and C6 were similar to the one of Column C4. The resulting natural period of the first mode was 5.13, 4.18, and 3.65 ms for Columns C4, C5, and C6, respectively.

To solve the nonlinear equilibrium equation, the Krylov-Newton algorithm provided by OpenSees was used. It is an iterative incremental solver based on the modified Newton method with Krylov subspace acceleration to calculate the next time step. This algorithm gives relatively faster and more robust convergence, in general (Charlson and Miller 1994).

The first step of the fiber-based model analysis was to calibrate the model using the hysteretic material behavior of CFST columns. Here, quasi-static cyclic loading test data were used to verify the developed analytical model itself. Two CFST column specimens (CFST-34 and CFST-42) tested by Marson and Bruneau (2004) were used, and the analytically predicted behavior of these columns was compared with the experimentally obtained one. The comparison between the analytical and experimental hysteresis loops showed that the maximum base moment of CFST columns was predicted within 10% accuracy when the drift exceeded 2% with better than 5% accuracy from 3% drift to 5% drift, which was deemed satisfactory given that this calibration was performed on cyclic inelastic displacement histories having dozens of hysteretic loops (as typically used in such earthquake engineering tests), which challenged the numerical models more significantly than monotonically increasing lateral load application up to comparable drifts would have. Given that the rotations at the plastic hinges in the specimens obtained during the blast tests exceeded 2% drift, the fiber-based model was confidently used for the blast analyses, allowing useful comparisons between results obtained using various analysis methods. As shown later, model bias will also be quantified by comparing the results obtained when replicating parameters corresponding to the simplified analyses.

Applied Blast Loadings

Two profiles of blast loadings were applied in the blast pressure history analyses as shown in Fig. 3(c). One is (1) the uniformly distributed (UD)-equivalent pressures, and the other is (2) the actual pressure distributions. The UD-equivalent pressures were selected for comparison with the SDOF dynamic analyses, which also used UD-equivalent pressures. Analyses using the UD pressures also provide some preliminary basic understanding of the column response subjected to blast loading. The equivalent pressure histories used here are identical to those used in the SDOF dynamic analyses. The analyses conducted using UD-equivalent pressures were only performed for the three test cases with midheight explosions (Test 3 on Column C4, Test 4 on Column C6, and Test 5 on Column C5), because the pressures actually applied to these columns during the tests were closer to symmetrically loading to the structure and are suited for modeling using UD loads due to this symmetry.

The actual pressure profiles were also calculated by BEL. The blast pressures were obtained at 84 data points along the height of a column, and these pressures were averaged within each member (approximately five pressure points with each member) to reduce computational time. Fig. 5 shows the resulting applied blast pressures for Test 3 as an example. Fig. 5(a) presents a comparison of the blast pressure distributions along the height at two selected different times ($t = 0.12$ and 0.25 ms) from BEL compared with those applied in the analyses, and Fig. 5(b) shows the applied pressure histories for two selected elements, which are Elem 1 and 8. This comparison indicates that the resolution of the averaged pressures within each member is satisfactory in terms of calculating the structural response. Note that the time in these figures starts at the initiation of the explosions. Also, note that a symmetric distribution of pressures is applied to the column, as shown in Fig. 5(a1), until the pressures are reflected on the ground. The reflected pressures on the ground are observed as higher pressures in the bottom elements, as shown in Fig. 5(a2).

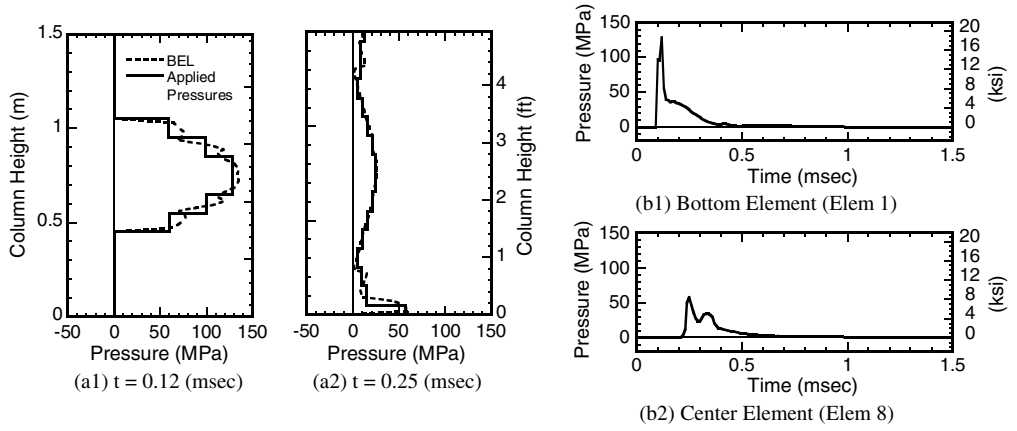

Fig. 5. Applied blast pressures for Test 3: (a) comparison of pressure distributions; (b) applied pressure histories

Structural Response of CFST Columns

Fig. 6 presents the analytical results of Test 3 for the midheight explosion case when subjected to the UD-equivalent pressures. These are acceleration and displacement distributions along the height of the column at three selected different times ($t = 0.12$, 0.60, and 1.04 ms). The time of 0.12 ms is shortly after the blast loading was applied, and the largest accelerations are observed at this time. Almost no deformation is observed along the column at this time. The times of 0.60 and 1.04 ms, are arbitrarily selected to show that high-frequency modes have developed in the acceleration response curves, similar to the mode shapes of the third and fifth modes, respectively, as shown in Fig. 4.

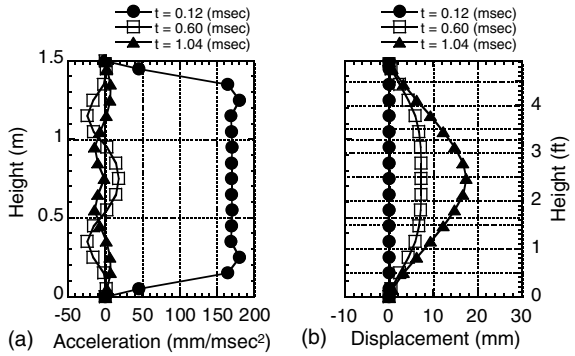

Fig. 6. Structural response distributions of Test 3 along height subjected to equivalent uniform pressures: (a) acceleration distribution; (b) displacement distribution

Fig. 7(a) compares the displacement history at midheight under the UD-equivalent pressures and actual pressures. In Fig. 7(a), when subjected to the UD-equivalent pressures, the maximum displacement of 41.8 mm is observed at a time of 4.02 ms, of course much later than the end of the applied blast pressures (the blast pressure starts at a time of 0.10 ms, and the pressure duration is 0.16 ms). The displacement history subjected to the actual pressures is similar to the one observed in the UD-equivalent pressure case. The reaction force history at the base and top of the column is shown in Figs. 7(b1) and (b2), subjected to the UD-equivalent pressures and actual pressures, respectively. As shown in Fig. 7(b1), the maximum reaction force of −303.8 kN is observed at a time of 0.15 ms that occurs before the end of the applied blast pressures. Note that the reaction forces at the base and top of the column are identical due to the symmetry of the column and applied blast pressure profiles. In Fig. 7(b1), there are some localized fluctuations of the reaction forces in the overall reaction force history curve. This is attributed to the high-frequency modes of vibrations. For instance, the localized fluctuation of the reaction forces observed around a time of 0.60 ms in Fig. 7(b1) is caused by the acceleration shape at the time of 0.60 ms in Fig. 6(a). As shown in Fig. 7(b2), when subjected to the actual pressures, the reaction forces at the base and top of the column are identical up to 0.23 ms, but after that, the magnitude of the reaction force at the bottom increases significantly due to the reflected pressures on the ground applied around low height of the column as shown in Fig. 5(a2).

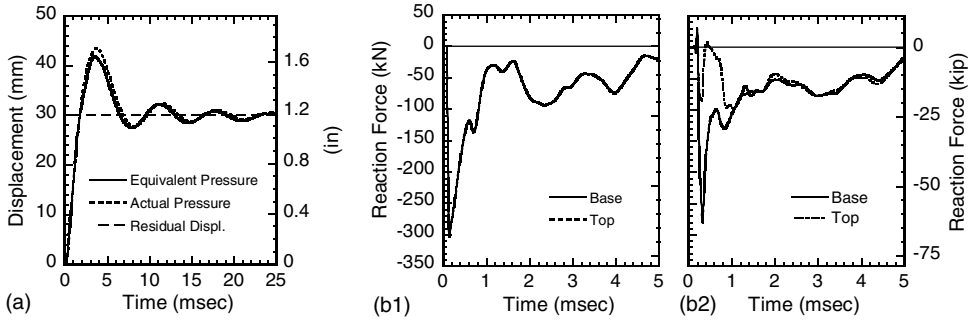

Fig. 7. Analytical results of Test 3 subjected to equivalent uniform and actual pressures: (a) comparison of displacement history at midheight; (b) reaction force history subjected to (b1) equivalent uniform pressures and (b2) actual pressures

Shape Factor

The shape factor β was calibrated for the six columns to match the analytical results obtained from the fiber-based analyses with the experimental results. Table 4 summarizes the averaged resulting shape factor β. For results using equivalent pressures, the β values obtained from the analyses with a 0.5% damping ratio, in addition to the ones with a 5% damping ratio, are also presented in Table 4 to investigate the sensitivity of damping effects on the values of β. Because the analyses with a 0% damping ratio did not converge, a small damping ratio of 0.5% was used for this purpose.

The average β value of 0.547, obtained from the fiber-based model with a 0.5% damping ratio using the UD-equivalent pressures, is comparable to the one of 0.532 from the SDOF dynamic analyses with a 0% damping ratio using the two different load-mass factors corresponding to the different structural ranges (i.e., Case 3 in Table 4). The difference between these two β values is within 3% (which quantifies the model bias described earlier).

The β value increases significantly, by approximately 18%, for the fiber-based model with the increase of the damping ratio from 0.5 to 5% in the UD-equivalent pressure profiles as shown in Table 4. In contrast, the increase of the damping ratio from 0 to 5% did not affect the β value significantly in the SDOF dynamic analyses, as presented in Table 4. This is because the fiber-based analysis can take higher modes of vibrations into account by using Rayleigh damping. To investigate this, Fig. 8 compares (1) the displacement history at column midheight and (2) the reaction force history at column base corresponding to 0.5 and 5% damping ratios for the Test 3 case. Note that different β factors, namely 0.564 for 0.5% damping and 0.630 for 5% damping, were used for these analyses to match the analytical residual displacement with the one from the experiment, as shown in Fig. 8(a). As shown in Fig. 8(b), the resulting reaction force at the base of the column using a 0.5 damping ratio fluctuates with higher frequencies (i.e., at short periods in the range of 0.1–0.2 ms), whereas the reaction history curve using a 5% damping ratio is relatively smoother and has less effects of higher-frequency modes. Since the 5% Rayleigh damping was used based on the first and third modes of vibrations, the high-frequency modes above the third mode were less significant to the response. Therefore, using the Rayleigh damping in a fiber-based model has an effect and can significantly reduce the structural response when subjected to blast loading.

Beyond the above, it is also observed in Table 4 that using the actual pressure profile slightly increased the average β value by 4% over using the uniformly distributed equivalent pressures for the midheight explosion case. When using actual pressure profiles, the average β value for the low-height explosion cases is 15% smaller than that for the midheight explosion cases, whereas this difference was only 3% for the SDOF dynamic analyses (Case 4), as shown in Table 4. This could be partly attributed to the reflected pressures on the ground computed by BEL. BEL assumes that the pressure reflects on the ground perfectly, but this was not the case in the experiments. Accordingly, the reflected pressures applied to the column close to the ground could be overestimated, resulting in the lower values of β for the low-height explosion cases. In the SDOF dynamic analyses, this possible overestimation of the reflected pressures can be reduced in the process of calculating the equivalent pressures given by Eq. (4) because of the normalized deflected shape of the column assumed in the calculation.

The results from the above analysis approaches (i.e., simplified analysis, SDOF dynamic analysis, and fiber-based dynamic analysis) highlight the fact that the shape factor, principally intended to account for the reduction of blast pressures due to the circular shape of a column, is, in fact, unavoidably affected by some of the assumptions built in analytical models and methods applied. Therefore, it is important to use the value of β that corresponds to the assumptions and conditions used for each analytical method. These are summarized in Table 5 along with the resulting β values for each analytical method considered here. Note that the β values are also affected by the accuracy of analytical models, and that backward verification of models to replicate results obtained with, the simpler one is important (as done here to determine moment capacity with the fiber-based analyses).

Finally, it is instructive to compare the β factor with the shape factor calculated from the drag coefficient for blast and from the pressures of wind loading. The drag coefficient, C_D, is used to calculate the transverse pressure on an object during passage of a blast wave. This coefficient is dependent on the shape of the object and can be found in the literature (e.g., Baker et al. 1983). By taking the ratio of the drag coefficient of a circular cylinder to that of a long rectangular member, the shape factor for the circular cylinder becomes $1.20/2.05 = 0.59$. For wind loading, the total force on a cylinder could be calculated by $F = q_z G C_f A_f$, where q_z = velocity pressure evaluated at height z; G = gust-effect factor; C_f = is the force coefficients; and A_f = projected area normal to the wind (ASCE 2006). There is a direct analogy between the β value and the factor C_f used to calculate wind forces. By linearly interpolating the tabulated values in ASCE (2006), C_f values of 0.64, 0.63, and 0.62 are, respectively, obtained for Columns C4, C5, and C6 (or 0.63, on average). Therefore, the values accounting for the shape of circular columns for drag pressure and for wind load, in this case, are approximately 0.59 and 0.63, respectively, which are close to the value of 0.61 obtained from the fiber-based dynamic analysis.

It is recognized that parameters such as pressure and impulse vary with scaled distance, contrary to other loads, such as wind

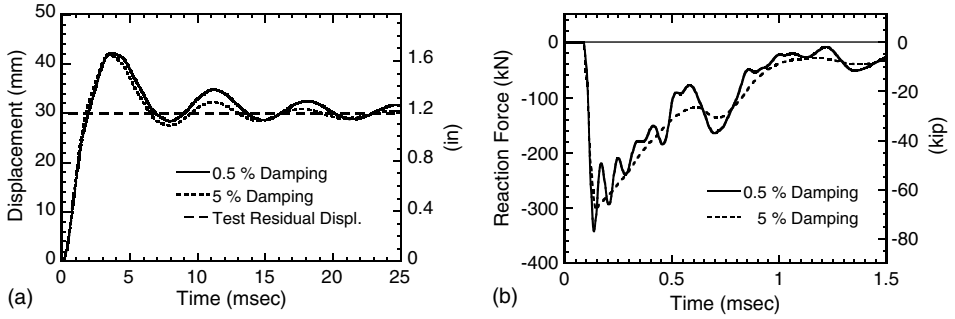

Fig. 8. Comparison of analytical results of Test 3 with different damping ratio: (a) displacement histories at midheight; (b) reaction force histories at base

Table 5. Summary of β Values and Assumptions of Each Analytical Method

	Assumptions and conditions	Simplified analysis	SDOF dynamic analysis	Fiber-based dynamic analysis
β Value	Midheight	0.46	0.54	0.67
	Low height	0.44	0.53	0.56
	All average	0.45	0.53	0.61
Modeling considerations	Column shape	Circular shape		
	Dynamic increase factor	Concrete strength: 1.25; steel yield stress: 1.20		
	Discretization of column	SDOF model		2D Fiber-based model
	Load-mass factor	$K_{LMe} = 0.66$ $K_{LMp} = 0.66$	$K_{LMe} = 0.775$ $K_{LMp} = 0.66$	No need
	Damping	Neglected	5% Viscous damping	5% Rayleigh damping
Blast loading considerations	Physical quantity	Impulse	Pressure	
	Applied loading	Equivalent impulse	Uniform equivalent pressure history	Actual pressure profile history

pressures. The results that have been presented here are for close-range blast (typically when the target is engulfed in the fireball). Future research at a different scaled distance is desirable to establish an appropriate range of applicability. Also, note that those results have been verified with experimental data obtained at 1/4 scale. Similar experiments should be conducted at larger scales for the same scaled distance to further validate the β values presented here. However, note that scale testing has gained substantial acceptance in blast engineering over the past decade and was proven to provide reliable results and key knowledge in understanding the behavior of structures subjected to blast (e.g., Woodson and Baylot 1999; Williams et al. 2008; Dr. J. Ray, personal communication, 2008; to name a few).

Conclusions

This study has showed that different values of β (which reduces blast pressures when applied to a circular column) must be used with different analytical methods. The assumptions and conditions that affect the values of β have been presented, and results have been summarized in Table 5. It was also noted that the structural response calculated using SDOF dynamic analyses was sensitive to assumptions in the load-mass factors selected to model structural components as an equivalent SDOF system; load-mass factors dynamically changing to match the specific ranges of response should be used in SDOF dynamic analyses. Fiber-based dynamic analyses showed that high-frequency modes of vibration have some influence on the structural response when subjected to blast loading. It was also found that using Rayleigh damping with the fiber-based model can significantly reduce the structural response under blast loading due to the high-frequency mode effects.

Future Research

Here, uniaxial constitutive models calibrated to quasi-static loading results were adopted by simply multiplying strength by dynamic increase factors. Research should investigate whether different uniaxial constitutive models are needed for confined concrete and steel subjected to impulsive loading to model uniaxial material behavior in fiber-element analyses. Detailed three-dimensional (3D) finite element models could be also developed for CFST columns to further investigate their ultimate behavior, such as local buckling or fracture of steel tubes. Future research at different scaled distances is desirable to establish an appropriate range of applicability. Likewise, similar experiments should be conducted at larger scales for the same scaled distance to further validate the β values obtained here.

Acknowledgments

This research was conducted by the University at Buffalo and was supported by the Federal Highway Administration under contract number DTFH61-98-C-00094 to the Multidisciplinary Center for Earthquake Engineering Research. This support is gratefully appreciated. However, any opinions, findings, conclusions, and recommendations presented in this paper are those of the writers and do not necessarily reflect the views of the sponsors. The authors especially thank Dr. James C. Ray at the Engineering Research and Development Center of the USACE for his help and assistance in the logistics of the experiments.

References

American Association of State Highway and Transportation Officials (AASHTO). (2009). *AASHTO LRFD bridge design specifications* (SI units, 4th Ed.), Washington, DC.

American Institute of Steel Construction (AISC). (1999). *LRFD specifications for structural steel buildings*, Chicago.

ASCE. (2006). "Minimum design loads for buildings and other structures." *ASCE/SEI 7-05*, Reston, VA.

Baker, W. E. (1973). *Explosions in air*, Univ. of Texas Press, Austin, TX.

Baker, W. E., Cox, P. A., Westine, P. S., Kulesz, J. J., and Strehlow, R. A. (1983). *Explosion hazards and evaluation*, Elsevier, Amsterdam.

Biggs, J. M. (1964). *Introduction to structural dynamics*, McGraw-Hill.

Bridge Explosive Loading version 1.1.0.3 (BEL) [Computer software]. U.S. Army Corps of Engineers, Engineer Research and Development Center, Vicksburg, MS.

Bruneau, M., and Marson, J. (2004). "Seismic design of concrete-filled circular steel bridge piers." *J. Bridge Eng.*, 9(1), 24–34.

Chai, Y. H., Priestley, M. J. N., and Seible, F. (1991). "Flexural retrofit of circular reinforced concrete bridge columns by steel jackets." *Rep. No. SSRP-91/06*, Dept. of Applied Mechanics and Engineering Sciences, Univ. of California, San Diego, CA.

Chang, G. A., and Mander, J. B. (1994). "Seismic energy based fatigue damage analysis of bridge columns: Part i—evaluation of seismic capacity." *Tech. Rep. NCEER-94-0006*, National Center for Earthquake Engineering Research, State Univ. of New York at Buffalo, Buffalo, New York.

Charlson, N. N., and Miller, K. (1994). "Design and application of a gradient-weighted moving finite element code part I: In 1-D." *J. Sci. Comput.*, 19(3), 728–765.

Commission of the European Communities. (1994). "Design of composite steel and concrete structures." *Eurocode 4*, Brussels.
Fujikura, S., and Bruneau, M. (2011). "Experimental investigation of seismically resistant bridge piers under blast loading." *J. Bridge Eng.*, 16(1), 63–71.
Fujikura, S., Bruneau, M., and Lopez-Garcia, D. (2007). "Experimental investigation of blast performance of seismically resistant concrete-filled steel tube bridge piers." *Tech. Rep. MCEER-07-0005*, MCEER, Univ. at Buffalo, Buffalo, NY.
Fujikura, S., Bruneau, M., and Lopez-Garcia, D. (2008). "Experimental investigation of multihazard resistant bridge piers having concrete-filled steel tube under blast loading." *J. Bridge Eng.*, 13(6), 586–594.
Marson, J., and Bruneau, M. (2004). "Cyclic testing of concrete-filled circular steel bridge piers having encased fixed-based detail." *J. Bridge Eng.*, 9(1), 14–23.
Mays, G. C., and Smith, P. D. (1995). *Blast effects on buildings*, Telford, London.
Menegotto, M., and Pinto, P. (1973). "Method of analysis for cyclically loaded RC plane frames including changes in geometry and non-elastic behavior of elements under combined normal force and bending." *Proc., Symp. Resistance and Ultimate Deformability of Structures Acted on by Well-Defined Repeated Loads*, Vol. 13, IABSE Reports, Lisbon, Portugal.
NONLIN Version 6.01 [Computer software]. Advanced Structural Concepts, Golden, CO.
OpenSees Version 1.7.5 [Computer software]. Pacific Earthquake Engineering Research Center, Univ. of California, Berkeley, CA.
Single-Degree-of-Freedom Blast Effects Design Spreadsheets (SBEDS) Version 3.1 [Computer software]. U.S. Army Corps of Engineers (USACE), Omaha, NE.
Spacone, E., Filippou, F. C., and Taucer, F. F. (1996a). "Fiber beam-column model for non-linear analysis of R/C frames: Part i. Formulation." *Earthquake Eng. Struct. Dyn.*, 25(7), 727–742.
Spacone, E., Filippou, F. C., and Taucer, F. F. (1996b). "Fiber beam-column model for non-linear analysis of R/C frames: Part ii. Applications." *Earthquake Eng. Struct. Dyn.*, 25(7), 711–725.
SPAn32 Version 1.2.7.2 [Computer software]. U.S. Army Corps of Engineers (USACE), Omaha, NE (distribution limited to U.S. Government agencies and their contractors).
U.S. Army Corps of Engineers (USACE). (2006). *User's guide for the single-degree-of-freedom blast effects design spreadsheets (SBEDS)*, Protective Design Center, Omaha, NE.
Williams, D., Holland, C., Williamson, E., Bayrak, O., Marchand, K., and Ray, J. (2008). "Blast-resistant highway bridges: Design and detailing guidelines." *Proc., 10th Int. Conf. on Structures under Shock and Impact (SUSI)*, WIT Press, Southampton, UK.
Winget, D. G., Marchand, K. A., and Williamson, E. B. (2005). "Analysis and design of critical bridges subjected to blast loads." *J. Struct. Eng.*, 131(8), 1243–1255.
Woodson, S. C., and Baylot, J. T. (1999). "Structural collapse: Quarter-scale model experiments." *Tech. Rep. No. SL-99-8*, U.S. Army Engineer Research and Development Center, Vicksburg, MI.